AGU PUBLICATIONS

JGR

Journal of Geophysical Research: Oceans

RESEARCH ARTICLE

10.1002/2013JC009705

Key Points:
- We use an objective method for parameter calibration in an ocean-sea ice model
- Simulation of ice dynamics is improved with the new parameters
- The method can be easily extended to GCMs applications

Correspondence to:
F. Massonnet,
francois.massonnet@uclouvain.be

Citation:
Massonnet, F., H. Goosse, T. Fichefet, and F. Counillon (2014), Calibration of sea ice dynamic parameters in an ocean-sea ice model using an ensemble Kalman filter, *J. Geophys. Res. Oceans*, *119*, 4168–4184, doi:10.1002/2013JC009705.

Received 7 DEC 2013
Accepted 16 JUN 2014
Accepted article online 18 JUN 2014
Published online 8 JUL 2014

Calibration of sea ice dynamic parameters in an ocean-sea ice model using an ensemble Kalman filter

F. Massonnet[1], H. Goosse[1], T. Fichefet[1], and F. Counillon[2]

[1]Georges Lemaître Centre for Earth and Climate Research, Earth and Life Institute, Université Catholique de Louvain, Louvain-la-Neuve, Belgium, [2]Mohn-Sverdrup Center for Global Ocean Studies and Operational Oceanography, Nansen Environmental and Remote Sensing Center, Bergen, Norway

Abstract The choice of parameter values is crucial in the course of sea ice model development, since parameters largely affect the modeled mean sea ice state. Manual tuning of parameters will soon become impractical, as sea ice models will likely include more parameters to calibrate, leading to an exponential increase of the number of possible combinations to test. Objective and automatic methods for parameter calibration are thus progressively called on to replace the traditional heuristic, "trial-and-error" recipes. Here a method for calibration of parameters based on the ensemble Kalman filter is implemented, tested and validated in the ocean-sea ice model NEMO-LIM3. Three dynamic parameters are calibrated: the ice strength parameter P^*, the ocean-sea ice drag parameter C_w, and the atmosphere-sea ice drag parameter C_a. In twin, perfect-model experiments, the default parameter values are retrieved within 1 year of simulation. Using 2007–2012 real sea ice drift data, the calibration of the ice strength parameter P^* and the oceanic drag parameter C_w improves clearly the Arctic sea ice drift properties. It is found that the estimation of the atmospheric drag C_a is not necessary if P^* and C_w are already estimated. The large reduction in the sea ice speed bias with calibrated parameters comes with a slight overestimation of the winter sea ice areal export through Fram Strait and a slight improvement in the sea ice thickness distribution. Overall, the estimation of parameters with the ensemble Kalman filter represents an encouraging alternative to manual tuning for ocean-sea ice models.

1. Introduction

Sea ice influences the climate system by moderating the exchanges of heat, mass, and momentum between the atmosphere and the oceans at high latitudes [*Thomas and Dieckmann*, 2010]. It is thus important that Earth System and General Circulation models (ESMs and GCMs) simulate the sea ice state as realistically as possible [*Notz*, 2012]. Sea ice models have considerably evolved over the past decades in their thermodynamic and dynamic components [*Hunke et al*., 2010] and will probably continue to do so in the future, e.g., by the inclusion of biogeochemical components [*Vancoppenolle et al*., 2013] or advanced sea ice rheologies [*Feltham*, 2008; *Girard et al*., 2011].

While higher model complexity can sometimes lead to improved sea ice simulations [*Massonnet et al*., 2011], it also has a price: as sea ice models include more processes, new parameters come into play and need to be adjusted. Manual tuning will soon become cumbersome (if not impossible), since the number of possible combinations of parameter values increases exponentially with the number of parameters to constrain. The methods to select the ultimate parameter values in sea ice models are rarely reported and not-well documented, a characteristic that had already been noted for ESMs and GCMs by *Mauritsen et al*. [2012]. This critical step of parameter calibration cannot be overlooked, given that simulated sea ice properties are strongly affected by the values attributed to several sea ice thermodynamic and dynamic parameters [e.g., *Shine and Henderson-Sellers*, 1985; *Fichefet and Morales Maqueda*, 1997; *Kim et al*., 2006; *Uotila et al*., 2012; *Dorn et al*., 2007; *Juricke et al*., 2012; *Rae et al*., 2014].

To the best of our knowledge, very few studies have attempted to optimize sea ice parameters in a systematic way. *Miller et al*. [2006] optimized three sea ice parameters in a stand-alone sea ice model. Using a brute-force method, they routinely scanned all possible triplets of these parameters to minimize a cost function based on a variety of sea ice observations. *Uotila et al*. [2012] explored the sensitivity of Arctic and Antarctic sea ice characteristics to several sea ice parameters, and again determined a set of optimal

© 2014. American Geophysical Union. All Rights Reserved.

parameters by running the model with all possible combination of the parameters. *Nguyen et al*. [2011] derived a cost function based on the linearization of a regional Arctic ocean-sea ice model. The 16 parameters were simultaneously tuned, leading to a reduction in model error by 45%. Finally, *Sumata et al*. [2013] compared two algorithms for parameter optimization in their regional ocean-sea ice model of the Arctic. Focusing on the year 2003, they reported a reduction of model-data misfit for this year after applying an optimization method derived from microgenetic algorithms.

Following the same goal as those previous studies, we implement in this paper a simple and objective method for parameter calibration adapted to large-scale sea ice models. The method is based on the ensemble Kalman filter (EnKF), in which parameters are treated as passive model variables [e.g., *Anderson*, 2001; *Annan et al*., 2005]. We focus our analysis on the Arctic sea ice drift characteristics of the global ocean-sea ice model NEMO-LIM3 [*Madec*, 2008; *Vancoppenolle et al*., 2009]. This model simulates reasonably well the sea ice areal and thickness distribution of the Arctic ice cover. However, like many GCMs, it is not able to capture in its default configuration the high-frequency variability of Arctic sea ice drift (daily fluctuations and spatial variability). We successfully implement in this study a method to calibrate sea ice dynamic parameters and improve the representation of sea ice drift statistics.

The remaining of the paper is structured in four parts. In section 2, we introduce the tools necessary for parameter calibration: a model (here NEMO-LIM3), a set of observations that guides the calibration of parameters (here observations of sea ice drift), and a statistical method for calibration (here a state-augmented version of the EnKF). In section 3, we demonstrate the efficiency of the EnKF scheme in idealized, twin experiments. We also report the results of parameter calibration when real observations are used. We interpret, analyze, and discuss in section 4 the impact of these new parameter values on the model simulations. The paper closes with a conclusion and recommendations.

2. Tools

We introduce in this section the ocean-sea ice model NEMO-LIM3 in its reference configuration. We identify a systematic underestimation of sea ice speed in the model at the daily time scale. We therefore develop a state-augmented version of the ensemble Kalman filter (EnKF) to calibrate sea ice dynamic parameters, given observations of sea ice drift.

2.1. Ocean-Sea Ice Model

NEMO-LIM3 is the acronym used to refer to the coupling between the global oceanic GCM OPA9 [*Madec*, 2008] and the sea ice model LIM3 [*Vancoppenolle et al*., 2009].

OPA9 is a finite difference, hydrostatic, primitive equation oceanic GCM typically designed for climate studies. In the present configuration, OPA runs on the ORCA2 grid ($\sim 2^\circ$ resolution) with mesh refinement around the equator and at the poles. In the Arctic basin, the grid cell edge length is typically $\sim$90 km. The vertical grid contains 31 levels and the first level is 10 m thick. Surface boundary layer mixing and interior vertical mixing are parameterized following a turbulent kinetic energy closure scheme based on the formulation of *Bougeault and Lacarrere* [1989] implemented by *Blanke and Delecluse* [1993] in OPA. The bottom boundary layer parameterization is based on *Beckmann and Döscher* [1997]. The reader is redirected to *Madec* [2008] for a detailed description of OPA.

LIM3 (Louvain-la-Neuve sea ice model, version 3) is a comprehensive sea ice model [*Vancoppenolle et al*., 2009]. The model explicitly resolves the subgrid-scale sea ice thickness distribution with five ice categories. It includes five vertical layers of ice and one of snow. Parameterization of brine entrapment and drainage processes allows for space and time variability of the salinity profile in the ice. Regarding dynamics, the C-grid formulation [*Bouillon et al*., 2009] of the elastic-viscous-plastic sea ice rheology (EVP) [*Hunke and Dukowicz*, 1997] is used.

The ice and ocean components, together referred to as NEMO-LIM3 from now, are coupled following the formulation of *Goosse and Fichefet* [1999]. NEMO-LIM3 is forced by daily 2 m air surface temperatures and (u, v) 10 m wind speeds from the NCEP/NCAR reanalysis project [*Kalnay et al*., 1996]. Monthly climatologies of relative humidity [*Trenberth et al*., 1989], total cloudiness [*Berliand and Strokina*, 1980], and precipitation [*Large and Yeager*, 2004] complete the atmospheric forcing of the model. We follow the formulation

© 2014. American Geophysical Union. All Rights Reserved.

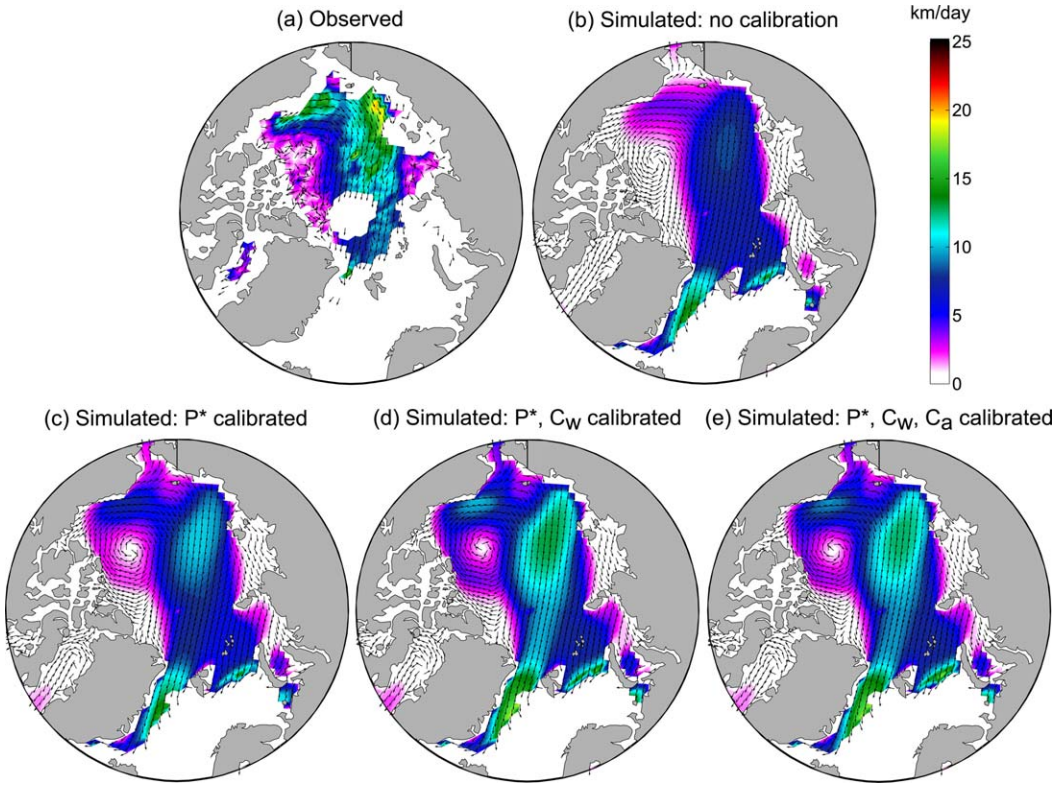

Figure 1. (a) Observed [*Lavergne et al.*, 2010] and (b–e) simulated mean sea ice drift for the period 12–14 April 2012. Sea ice drift is expressed in km/d. The drift magnitude is expressed by the color code, its direction by the arrows of normalized length.

described in *Goosse* [1997] to prescribe the atmosphere-sea ice and atmosphere-ocean turbulent and radiative heat fluxes. River runoff rates follow the climatological data set of *Baumgartner and Reichel* [1976] combined with a mean seasonal cycle derived from the Global Runoff Data Centre data [*GRDC*, 2000]. A weak restoring toward observed sea surface salinities of *Levitus* [1998] is applied, with a relaxation time scale of 1 year. The ocean time step is 5760 s (1/15 day) and the sea ice model is called every five ocean time steps.

2.2. Reference Configuration

Historically, NEMO-LIM3 sea ice dynamic parameters were tuned in a heuristic, "trial-and-error" process, with the goal to best match the ice areal export through Fram Strait (M. Vancoppenolle, personal communication, 2013). While sea ice extent and thickness are realistically simulated in the Arctic in the default configuration [*Vancoppenolle et al.*, 2009], the Arctic sea ice drift simulated at the daily time scale exhibits clear biases. Figure 1a is a snapshot of observed sea ice motion observed during a 2 day period in April 2012. Because NEMO-LIM3 is forced by atmospheric reanalyzes, it is expected to reproduce this motion. The direction of the flow is simulated overall correctly, but its intensity clearly is not (Figure 1b). In addition, sea ice is nearly motionless in a large portion of Beaufort Sea and the gradients of sea ice velocity are clearly too smooth compared to observations. At the model's resolution, oceanic eddies are not explicitly represented and their effect is instead parameterized in terms of global state variables [*Madec*, 2008]. The fact that the modeled drift is globally too slow may be in part attributed to this issue, but this is probably not the only reason.

Deficiencies in the simulation of Arctic sea ice drift, and subsequently deformation, can be problematic. During winter, in regions of strong ice divergence, the ice pack cracks. Significant amounts of sensible and latent heat escape from the ocean to the atmosphere [*Thorndike et al.*, 1975]. The production of new ice is accompanied by a significant release of brine altering the global ocean freshwater budget. In spring and summer, the fracturing of ice decreases the local albedo [*Girard et al.*, 2009], with possible positive feedbacks on the polar atmosphere. In areas of ice convergence, rafting and ridging processes modify the subgrid-scale distribution of sea ice thickness, which is of particular relevance for seasonal prediction

© 2014. American Geophysical Union. All Rights Reserved.

[*Chevallier and Salas Mélia*, 2012]. Finally, sea ice drift governs the advection of the main sea ice properties, including volume. Biases in the simulated sea ice drift may thus induce incorrect spatial patterns of sea ice thickness.

In LIM3, as in many other large-scale sea ice models, the change in sea ice velocity **u** of a sea ice element of mass *m* per unit area is deduced from the momentum balance (the advection term is neglected; at the time and spatial scales of interest, it is indeed small in comparison to the other terms [*Vancoppenolle et al.*, 2009]):

$$m\frac{\partial \mathbf{u}}{\partial t}=-mf\mathbf{k}\times\mathbf{u}-mg\nabla\eta+\tau_a+\tau_w+\nabla\cdot\boldsymbol{\sigma} \tag{1}$$

The first term in the right-hand side of equation (1) is the Coriolis force: **k** is a unit vector pointing normal to the surface and *f* is the Coriolis parameter. The term $-mg\nabla\eta$ is the force due to sea surface tilt: $g=9.81$ m s^{-2} is the acceleration of gravity and η is the sea surface elevation. The terms τ_a and τ_w are the atmospheric and oceanic stresses on the sea ice element, respectively. They depend on the strength and direction of wind and ocean currents, respectively, but also on the way sea ice interacts with them through the boundary layer. Finally, the term $\nabla\cdot\boldsymbol{\sigma}$ accounts for all internal forces. In the Arctic Ocean, the acceleration term is negligible for time scales greater than a day [*Leppäranta*, 2005], the Coriolis and sea surface tilt contributions are small but their combined contribution is even smaller [*Steele et al.*, 1997]. Thus, the three last terms of equation (1) actually dictate sea ice motion. The modeled sea ice velocity is thus controlled mainly by (1) the way the atmosphere-sea ice interactions are formulated, (2) the way ocean-sea ice interactions are formulated, and (3) the way internal sea ice forces are formulated.

The transfers of momentum between the atmosphere/ocean and sea ice are parameterized in NEMO-LIM3 as

$$\tau_a=\rho_a C_a|\mathbf{u}_a|\mathbf{u}_a$$
$$\tau_w=\rho_w C_w|\mathbf{u}_w-\mathbf{u}|(\mathbf{u}_w-\mathbf{u})$$

with ρ_a (ρ_w) the air (seawater) density in the boundary layer and $\mathbf{u}_a$ ($\mathbf{u}_w$) the wind velocity at 10 m from atmospheric reanalyzes (ocean velocity in the first ocean layer). The dimensionless proportionality constants C_a and C_w, often referred to as the atmospheric and oceanic-sea ice drag coefficients, respectively, thus clearly appear as good candidates for parameter calibration for sea ice drift.

Regarding internal forces, a key parameter central to the (E)VP rheology is the so-called ice strength parameter P^* and relates sea ice strength *P* to its compactness (concentration) *A* and mean thickness *h*. It was first introduced by *Hibler* [1979] in the constitutive equation for ice strength as

$$P=P^*h\exp\left(-C(1-A)\right) \tag{2}$$

In turn, sea ice strength *P* appears in the law relating sea ice strain rate to the internal stress tensor $\boldsymbol{\sigma}$. Thus, in Hibler's parameterization, sea ice offers less resistance to compression when P^* is low, and tends to pile up more easily because of enhanced mechanical ridging and rafting. Along with the atmospheric and oceanic drag coefficients, P^* has been identified as a critical parameter for sea ice dynamics [*Stössel et al.*, 1990; *Steele et al.*, 1997; *Owens and Lemke*, 1990; *Juricke et al.*, 2012].

Steele et al. [1997] conducted a budget analysis of the momentum balance (equation (1)) using an ocean-sea ice model. As stated above, only the three last terms of equation (1) are of significant importance at daily time scales. *Steele et al.* [1997] pointed out that, at such time scales, the momentum balance is dominated by two terms: either the air drag and internal stress gradient dominate (regime I) or the air drag and oceanic drag dominate (regime II). Regime I is typically found from fall to spring in the interior of the pack where the ice is compact. Regime II is found where sea ice is thinner and less concentrated. It is particularly frequent in summer, when internal forces play a less prominent role and sea ice is drifting almost freely. Accordingly, we can partition the approximate version of the momentum equation for Arctic sea ice drift into:

© 2014. American Geophysical Union. All Rights Reserved.

$$\begin{cases} \tau_a + \nabla \cdot \boldsymbol{\sigma} = 0 & \text{(regime I)} \\ \boldsymbol{\tau}_a + \boldsymbol{\tau}_w = 0 & \text{(regime II)} \end{cases} \tag{3}$$

Since the three parameters P^*, C_w, and C_a have a direct impact on $\nabla \cdot \boldsymbol{\sigma}$, τ_a, and τ_w, respectively, we choose this triplet of parameters as our calibration target for optimizing sea ice drift in the model.

2.3. Synthetic and Real Observations

We intend to calibrate three sea ice dynamic parameters. It is thus a natural choice to use observations of sea drift for that purpose. However, model-observation comparison should be carried out with extreme caution when it comes to ice drift. The Arctic sea ice velocity field is the result of synoptic-scale weather-induced sea ice motion superimposed on long-term fluctuations due to prevailing wind and ocean currents [*Thorndike*, 1986; *Rampal et al*., 2009]. Because the contributions from synoptic ice motion tend to cancel out at monthly time scales and beyond, a model evaluation based on its monthly sea ice motion could look correct, but for wrong reasons. We will therefore assess in the remainder of the text the ability of NEMO-LIM3 to model the observed sea ice motion field at the daily time scale.

For validation purposes detailed in section 3, we first constructed synthetic observations. That is, we first ran NEMO-LIM3 in its standard configuration with default parameters. We then stored as "observations" the (u, v)-components of the model ice velocity plus a Gaussian white noise with standard deviation equal to 1 cm/s (8.64 km/d).

For the actual parameter calibration step, we used the Ocean and Sea Ice Satellite Application Facility (OSI SAF) low-resolution sea ice drift product [*Lavergne et al*., 2010]. Sea ice displacement over successive 48 h time spans are derived from a Continuous Maximum-Cross-Correlation algorithm. This product shows no bias compared to in situ Geophysical Processor System (GPS) data [*Lavergne et al*., 2010]. The data are limited to the Arctic, from October to April and between 2007 and 2013. The retrieval of sea ice motion is not feasible between melt onset and freezeup due to atmospheric turbulence noise and surface melting [*Maslanik et al*., 1998]. The original drift product is provided on a 62.5 km by 62.5 km polar stereographic grid. We interpolated and aligned the two components of sea ice drift from this grid to the ORCA2 grid. Finally, we assigned to each model grid point and for each drift component an uncertainty equal to the standard deviation of the spatial distribution of this component (representativeness error).

2.4. Parameter Estimation With the EnKF

The ensemble Kalman filter [*Evensen*, 2003] is a sequential data assimilation technique often applied in geophysical studies [*Evensen*, 2007]. The main advantage of the EnKF lies in the representation of the model error covariance matrix. This matrix is approximated by the sample covariance of a number of model forecasts, typically 10–100, supposed to sample the model uncertainty. In addition, no linearization of the model operator is required, as is the case in adjoint methods or in the extended Kalman filter. The estimation of state returned by the EnKF is a minimum variance estimate, and coincides with the maximum likelihood (Bayesian) if model and observational error distributions are Gaussian and centered around zero [e.g., *Jazwinski*, 1970].

For sea ice, the EnKF has mostly been used so far for state estimation [*Lisæter et al*., 2003, 2007; *Mathiot et al*., 2012; *Massonnet et al*., 2013]. Estimating the state is interesting to reconstruct the history of a system or to initialize short-term predictions. However, the model will drift back toward its preferred climatology as soon as observations are not available to constrain the model. In that respect, parameter estimation is an alternative solution to adjust indirectly the climate of a model [*Annan et al*., 2005] without updating explicitly its state during the assimilation. Parameter estimation can be performed in the same theoretical framework as state estimation, by augmenting the state vector by the few parameters that need to be estimated.

The EnKF scheme consists in two sequential steps: forecast and analysis.

1. *Forecast*. An ensemble of $N = 25$ members is propagated in time, here for a period of 15 days. Each member runs with a perturbed version of the atmospheric forcing in order to account for model uncertainty and maintain sufficient spread in the ensemble (see *Mathiot et al*. [2012] for details about the perturbation method). In addition, each member runs with different parameter values, in order to estimate the effect of the parameters to be calibrated on the model state. Let then

© 2014. American Geophysical Union. All Rights Reserved.

$$\mathbf{X}^f = [\mathbf{x}_1^f, \cdots, \mathbf{x}_N^f] \in \mathbb{R}^{n \times N}$$

be a matrix representation of these $N = 25$ forecasts, arranged vertically next to each other (the superscript f stands for "forecast"). That is, the ith column of $\mathbf{X}^f$ contains all sea ice and ocean prognostic variables from all model grid points for member i (except the sea ice heat content [*Mathiot et al.*, 2012; *Massonnet et al.*, 2013]), as well as the parameter values that have been used during the forecast of member i. The ensemble mean $\overline{\mathbf{X}^f}$, taken horizontally over the N members, is the best estimator of the model forecast. Likewise, the model error covariance matrix $\mathbf{P}^f$

$$\mathbf{P}^f = \frac{1}{N-1} \mathbf{X}^{f'} (\mathbf{X}^{f'})^T$$

can be used to approximate the true, unknown model forecast error and the relationship between parameters and model state variables. Here, the superscript T denotes matrix transpose, and $\mathbf{X}^{f'}$ is the matrix of model forecast anomalies obtained by subtracting $\overline{\mathbf{X}^f}$ from each column of $\mathbf{X}^f$.

2. *Analysis*. During the analysis step, the filter uses information from p observations stored in a vector $\mathbf{Y} \in \mathbb{R}^{p \times 1}$, with an error covariance matrix $\mathbf{R} \in \mathbb{R}^{p \times p}$. This allows to analyze, or "update," the model forecasts $\mathbf{X}^f$. Because we are performing *parameter* estimation, we do not update the state itself during the analysis; only the parameters are updated. We assume a diagonal structure for the matrix $\mathbf{R}$, i.e., uncorrelated observation errors.

For practical implementation and to avoid the use of perturbed observations required in the classical EnKF scheme [*Burgers et al.*, 1998], we follow here the deterministic formulation of the EnKF (DEnKF) [*Sakov and Oke*, 2008]. This scheme proceeds traditionally in two steps. First, the mean of the ensemble forecasts $\overline{\mathbf{X}^f}$ is updated:

$$\overline{\mathbf{X}^a} = \overline{\mathbf{X}^f} + \mathbf{K}(\mathbf{Y} - \mathbf{H}\overline{\mathbf{X}^f}) \tag{4}$$

In our particular case of parameter estimation, we only update the mean of the parameters, that is, the entries of $\mathbf{X}^f$ corresponding to parameters. In equation (4), the superscript ^{a} denotes "analysis," and $\mathbf{H} \in \mathbb{R}^{p \times n}$ is the matrix projecting the model prognostic variables to the measurements domain. In practice, $\mathbf{Y}$ contains observations of 2 day sea ice drift components interpolated and rotated onto the model grid, while $\mathbf{H}\overline{\mathbf{X}^f}$ contains the 2 day averaged model drift components at the same grid points. The Kalman gain $\mathbf{K}$ is computed as

$$\mathbf{K} = \mathbf{P}^f \mathbf{H}^T (\mathbf{H}\mathbf{P}^f \mathbf{H}^T + \mathbf{R})^{-1} \tag{5}$$

Then, the DEnKF updates the forecast anomalies in a way that the resulting covariance matrix matches the theoretical value, up to the truncation of quadratic or higher degree terms:

$$\mathbf{X}^{a'} = \mathbf{X}^{f'} - \frac{1}{2}\mathbf{K}\mathbf{H}\mathbf{X}^{f'} \tag{6}$$

Again, we only apply this step to the parameters and leave the model state variables unchanged.

The full set of analyzed parameters is finally reconstructed by adding the updated mean of parameters to each column of the matrix of updated parameter anomalies. If the update happens to produce negative values, then we reset the parameters to prescribed minimum values: 1000 N/m^2 for P^*, 0.1×10^{-3} for both C_w and C_a.

The trace of the covariance of the analyzed state vector is always reduced compared to that of the forecast state vector [*Burgers et al.*, 1998]. At the same time, the ensemble size (25 members) is relatively small and sampling errors are large. This leads then to an artificial reduction of the ensemble spread [see, for example, *Bocquet*, 2011]. An adhoc approach to handle this problem is to use multiplicative inflation [*Anderson*, 2001]. We therefore inflate the parameter spread by 20% after the analysis step.

© 2014. American Geophysical Union. All Rights Reserved.

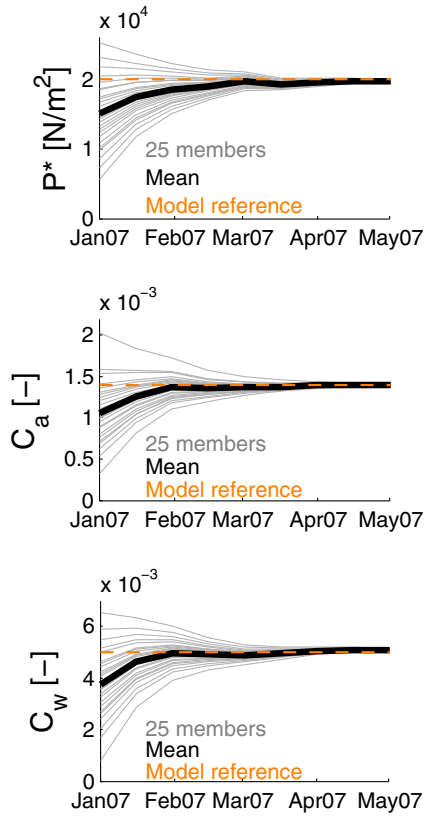

Figure 2. Convergence of parameters in twin experiments. The thin, gray lines represent the evolution in time of the three parameters of interest after the analysis step for the 25 members. The thick, black line is the mean taken over the 25 members. The dashed, orange lines are the reference values for the parameters (first row of Table 1).

We stop the parameter estimation when the standard deviation of the ensemble is less than 0.1% of the mean and take the mean parameter value at that time as the ultimate, calibrated value. It should be noted that an alternative approach could be to maintain the spread of the ensemble at constant value by adjusting the inflation parameter consequently. This could then provide a time-varying estimation of the optimal set of parameters [e.g., *Keghouche*, 2010]. In addition, we consciously designed the parameter estimation to be global. That is, we end up after calibration with one, space-independent value for each parameter.

3. Results of Parameter Calibration

In this section, we first apply the parameter calibration in an idealized framework. A reference simulation with known parameters is considered as the truth and is used as observations for the parameter estimation. In this idealized twin experiment, the goal is to retrieve the original set of parameters. We are able to do so within 1 year of simulation. We then run the parameter calibration scheme with real data of sea ice drift.

3.1. Twin Experiments

In order to test the validity of the method, we designed the following experiment. We drew parameter values for P^*, C_w and C_a from a multivariate Gaussian distribution, with means intentionally lower by 25% than in the reference configuration, and with a standard deviation equal to 33% of the mean. We then ran the parameter-estimation procedures described in section 2.4. No perturbation in the atmospheric boundary forcing was applied to ensure actual perfect-model conditions. Still, we perturbed the synthetic observations by adding a Gaussian white noise of standard deviation 1 cm/s at all ice covered grid points, as described in section 2.3.

In this three parameter joint estimation experiment, it takes about 1/2 year of simulation to retrieve the original set of parameters. Figure 2 depicts the evolution of the analyzed parameter ensemble for the three parameters P^*, C_w and C_a. As illustrated in this figure and in Table 1, the asymptotic values of those parameters are in close agreement with the target values (difference of 1% or less).

The method is successful from a "perfect-model" point of view. In other words, assuming that the sole source of model uncertainty lies in its parameters, then the EnKF parameter-estimation method converges to the reference triplet of parameters. We also conducted a twin experiment where we activated the perturbation in the atmospheric forcing (not shown here). In this case, the value for P^* after convergence was 1% less than the reference, but the values for C_w and C_a were each 20% below the reference. The ratio C_w/C_a remained, however, within 1% of the ratio of the reference parameters. This second twin experiment confirmed the statement that the ratio C_w/C_a is more important for sea ice drift than the individual absolute values for C_w and C_a [*McPhee*, 1980; *Stössel*, 1992; *Harder and Fischer*, 1999; *Fischer and Lemke*, 2013]. The

© 2014. American Geophysical Union. All Rights Reserved.

Table 1. Values of the Three Parameters of Interest After Convergence, i.e., When the Standard Deviation of the Ensemble is Less Than 0.1% of the Mean[a]

	P^* (10^4 N/m^2)	C_w (10^{-3})	C_a (10^{-3})
Reference	2.00	5.00	1.40
Twin	1.98	5.04	1.40
C1	1.04	–	–
C2	0.98	2.94	–
C3	1.28	3.78	1.64

[a]In the "Twin" experiment, we calibrated the three parameters using perturbed model output from the reference run, whose default parameters are reproduced in the top row. A dash "–" is used to mean that the parameter was not estimated and was locked to its default value. Note that the reference value for P^* is half of that used in *Vancoppenolle et al.* [2009] (40,000 N/m^2 in their paper): a inconvenient factor of 0.5 was discovered in the code since then, making the actual model reference equal to 20,000 N/m^2.

existence of a close relationship between optimal values for C_w and C_a is important to bear in mind, and we will get back to it later in this paper.

3.2. Real Experiments

A second set of experiments was then conducted in real conditions, that is, with assimilation of observed sea ice drift data [*Lavergne et al.*, 2010]. The calibration experiments all start in January 2007. We remind the reader that no sea ice drift data are available from May to September. We conducted three calibration experiments. In the first experiment, labeled C1, we estimate P^* only and leave C_w and C_a to their default values. We expect, from the analysis of the simplified momentum balance equation (3), that optimizing P^* will lead to improve sea ice drift in regime I. Then, in experiment C2, we calibrate both P^* and C_w as to also optimize sea ice drift for ice of type II. Finally, we calibrate in experiment C3 the three parameters P^*, C_w, and C_a together as to hopefully improve the simulation of sea ice drift even further. In all three experiments, the perturbation of the atmospheric boundary conditions (section 2.4) is enabled as it corresponds to a dominant source of error in a realistic framework.

Since no prior information about the optimal set of parameters is available, we drew the initial distribution of parameters from a Gaussian distribution with mean equal to the reference values (first row of Table 1) and with standard deviations for P^*, C_w, and C_a equal to $0.75\times10^4\mathrm{N/m^2}$, 1.5×10^{-3}, and 0.3×10^{-3}, respectively. The largest changes in parameter values occur during the first 4 months of estimation (January to April 2007, not shown here). In the second year, the means of the ensembles stabilize around their final values. The asymptotic values are reached in the beginning of 2009 or 2010. These asymptotic, calibrated values after estimation are reported in Table 1.

Based on the three calibration experiments C1, C2, and C3 in Table 1, we finally ran the three corresponding simulations over 2007–2012. The first simulation is identical to the reference NEMO-LIM3 simulation described in section 2.2, except that the value for P^* is now set to $1.04\times10^4\mathrm{N/m^2}$. The second simulation is identical to NEMO-LIM3 in the reference configuration, except that the values for P^* and C_w are set to $0.98\times10^4\mathrm{N/m^2}$ and 2.94×10^{-3}, respectively. The third and last simulation is identical to NEMO-LIM3 in its reference configuration, except that the values for P^*, C_w, and C_a are set to $1.28\times10^4\mathrm{N/m^2}$, 3.78×10^{-3}, and 1.64×10^{-3}, respectively. We discuss in the next sections the impact of these new sets of parameters on model results.

4. Discussion

We discuss in this section the impact of the new, calibrated parameter values of Table 1 on NEMO-LIM3 simulations. As explained at the end of the previous section, three 2007–2012 simulations were run with P^* calibrated only, (P^*, C_w) calibrated, and (P^*, C_w, C_a) all together calibrated. We first investigate the sensitivity of sea ice drift to this new set of parameters, and then discuss the implications for other sea ice variables.

4.1. Impact on the Simulated Sea Ice Drift

Without ambiguity, the impact of the new parameters on the simulated sea ice drift characteristics is positive. We first illustrate this by looking back at the 2 day sea ice motion snapshot that we used to highlight NEMO-LIM3 sea ice drift biases (Figure 1). We will present a more general diagnostic for the full 2007–2012 period in the next paragraph. The three simulations with calibrated parameters (Figures 1c–1e) clearly represent an improvement compared to the reference simulation (Figure 1b). As noted earlier, the direction of the motion is well represented in all simulations, but the way sea ice responds to the wind and ocean forcings appears largely sensitive to parameter values. A particular improvement lies in the range of speeds covered in the simulation with the new parameters. During the 2 day period of interest and wherever

© 2014. American Geophysical Union. All Rights Reserved.

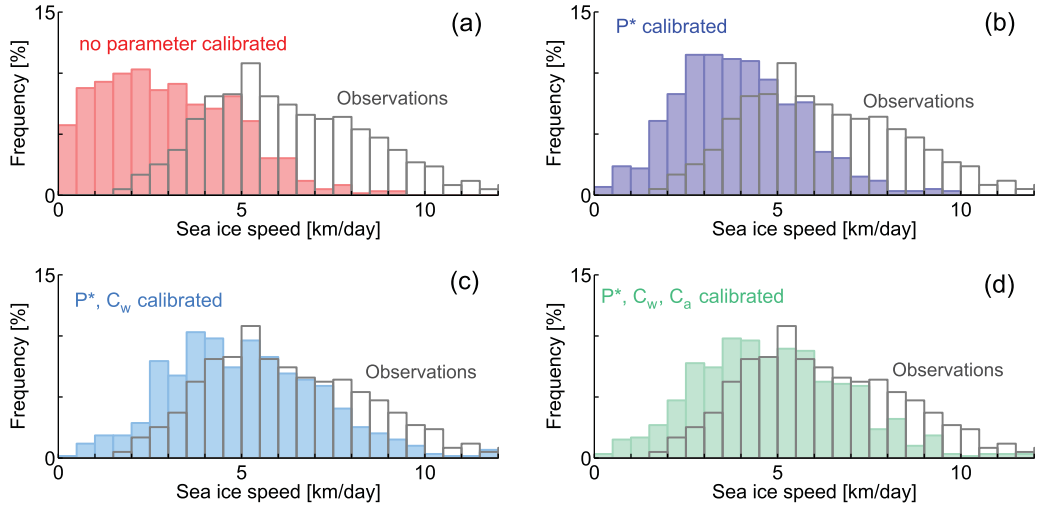

Figure 3. Distribution of the 2007–2012 simulated sea ice speeds (a) in the reference run and (b–d) after calibration of parameters. The observed frequencies [*Lavergne et al.*, 2010] are shown by the gray bars. For each 2 day period between 2007 and 2012 where both observations and model data were available, we first computed the median sea ice speed from the spatial field of Arctic sea ice drift, in observations and in the model restricted to the domain of observations (total: 592 data). With these 592 data available over 2007–2012, we then constructed the histograms between 2007 and 2012.

observations are available, sea ice actually drifts with speeds ranging from ~2 km/d (Beaufort Sea) to ~18 km/d (East Siberian Sea). NEMO-LIM3 in its reference version simulates ice speeds ranging from ~0 km/d to ~8 km/d, while the simulations with calibrated parameters show drifts ranging from ~3–4 km/d in the Beaufort Sea to ~10–15 km/d in the Eastern Siberian Sea, in better agreement with observations.

The maps in Figure 1 are insightful, but only show Arctic sea ice drift for a particular 2 day period. Therefore, for each 2 day period between 2007 and 2012 where both model and observations were available (592 time periods), we recorded the median speed from the spatial Arctic sea ice drift field. In Figure 3, we show the distribution of these 592 median speeds over 2007–2012. The median was chosen instead of the mean because the distribution can likely be skewed toward high values. The histograms of Figure 3 generalize the conclusions drawn from the maps of Figure 1 and reveal two interesting features. (1) The three simulations with calibrated parameters display sea ice speed distributions that are shifted toward higher and more realistic values than in the reference simulation. (2) There is a clear improvement from the reference simulation to the simulation with calibrated P^*; the additional calibration of the oceanic drag coefficient C_w improves even further the shape of the distribution. However, the estimation of C_a does not bring additional skill if P^* and C_w are already estimated.

To confirm the previous statement that the estimation of C_a is not necessary when P^* and C_w are already estimated, we looked at the difference in median sea ice speed between the observations and our simulations over 2007–2012 (Figure 4). Consistently with the previous diagnostics in Figure 3, the reference version of the model underestimates the observed sea ice speed all over the Arctic basin (Figure 4a). When P^* is calibrated, the bias in sea ice speed is reduced mostly in the interior of the ice pack. This is to be expected, because the parameterization in which P^* takes place involves an exponential function of one minus the ice concentration (equation (2)). At low sea ice concentration, say less than 90%, the changes in the parameter P^* do not have much direct impact on the ice drift. When both the oceanic drag C_w and P^* are calibrated, further improvements are noticed. The third simulation with calibrated P^*, C_w, and C_a does not further reduce the bias in simulated sea ice speed.

We propose to discuss the effect of estimation of successive parameters in light of the momentum budget analysis described in equation (3). When we calibrate P^* only and keep C_a and C_w equal to their default values, we find the value of P^* for which the model sea ice velocity is in best agreement with observations for regime I only, since the estimated parameter P^* has very little impact on ice dynamics in regime II. The error in the simulated drift can be further reduced if we proceed to the estimation of C_w, because C_w impacts ice dynamics mostly in regime II. The estimation of (P^*, C_w) yields indeed improved metrics compared to the run with estimation of P^* only (Figures 3 and 4). The additional estimation of C_a is then not necessary,

© 2014. American Geophysical Union. All Rights Reserved.

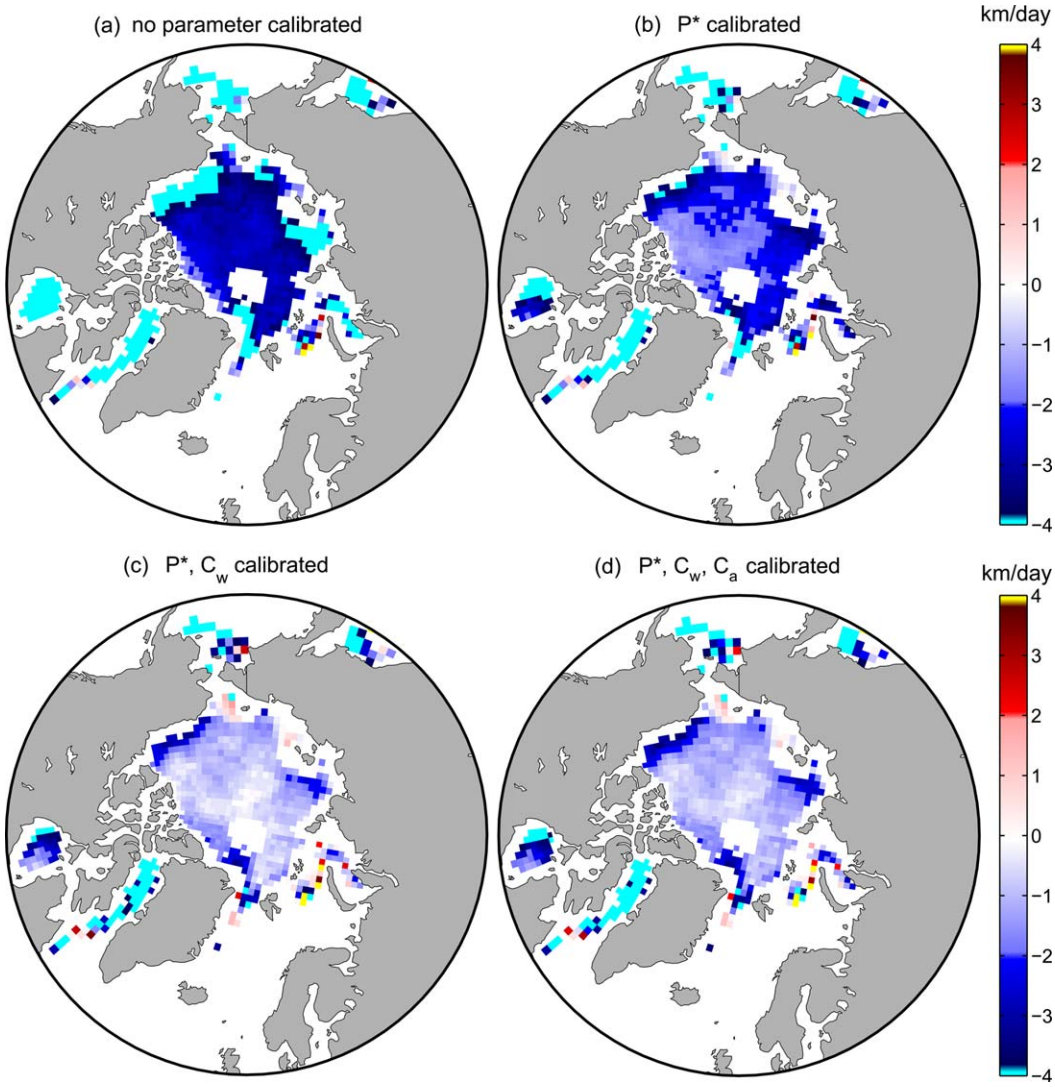

Figure 4. Difference between simulated and observed median sea ice speeds during the period 2007–2012 in (a) the reference run and (b–d) the simulations with calibrated parameters.

because the ice drift is already optimally constrained in regimes I and II separately by the estimation of the two parameters P^* and C_w, which control respectively ice dynamics in these two regimes. Another explanation why the estimation of C_a is not necessary is related to the fact that the ratio C_w/C_a is more important for ice drift than the individual absolute values [*McPhee*, 1980; *Stössel*, 1992; *Harder and Fischer*, 1999; *Fischer and Lemke*, 2013]. We have good reasons to believe that this is also the case in our ocean-sea ice model (see section 3.1). If the optimal parameter values for C_a and C_w are indeed related to each other by a constant ratio, then estimating one of the two parameters while keeping the other at constant value is sufficient to optimize the ice drift in our model.

From now on, we exclusively focus our analyses on the simulation with calibrated P^* and C_w, as it was found that calibrating these two parameters is sufficient to produce more realistic distributions of ice speed in the Arctic (Figure 3).

4.2. Impact on the Other Sea Ice Variables

Because sea ice dynamics and thermodynamics are intimately intertwined [e.g., *Hibler*, 1979], the change in dynamic parameters are likely to affect the sea ice variables other than drift. We present hereafter an overview of sea ice thickness, extent and export properties through Fram Strait for the simulation with calibrated P^* and C_w.

© 2014. American Geophysical Union. All Rights Reserved.

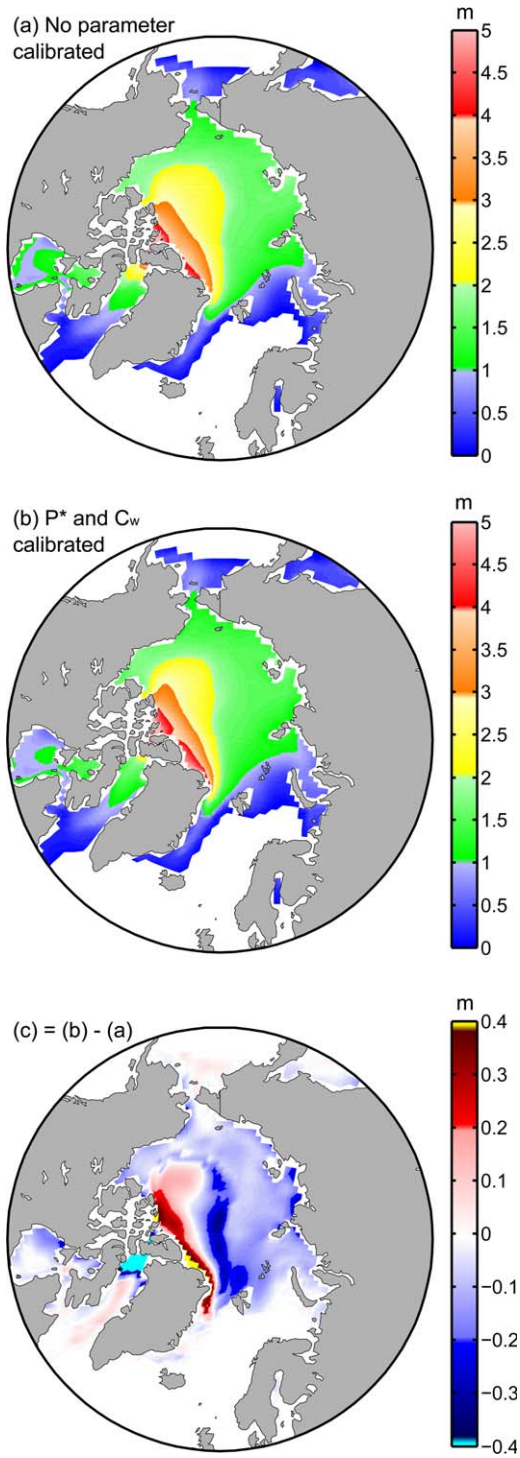

Figure 5. The 2007–2012 average Arctic sea ice thickness distribution in March from (a) the reference simulation and (b) the simulation with (P^*, C_w) calibrated. The thickness difference between the two simulations is shown in (c).

4.2.1. Impact on the Sea Ice Thickness Distribution

The distribution of ice thickness in the Arctic basin is sensitive to the changes in P^* and C_w. In Figure 5, we plot the simulated average sea ice thickness distribution for March 2007–2012. After calibration, the sea ice pack is globally thicker along the north coasts of Greenland and the Canadian Arctic Archipelago, and thinner elsewhere (Figure 5c). The gradient in ice thickness across the basin is stronger in the experiment with calibrated parameters. This was expected: since the value of P^* decreases from 2.00×10^4 to 0.98×10^4 N/m^2 after calibration, the ice becomes much less stiff and tends to pile up more easily in response to the prevailing winds. We also note a large reduction in sea ice thickness in the northern part of Baffin Bay, where sea ice is known to accumulate unrealistically in the reference configuration [*Vancoppenolle et al.*, 2009].

To gain a quantitative appreciation of these changes, we compare the simulated sea ice thickness with data from the Operation IceBridge campaigns [*Kurtz et al.*, 2013]. Since 2009, several airborne missions have been conducted in the Arctic. Laser altimetry techniques enabled to retrieve sea ice freeboard, and subsequently sea ice thickness along the tracks of the flights. We use the data from 35 campaigns between 2009 and 2012 for our assessment. For each campaign, we collocated the model and observational data by averaging the high-resolution measurements in each grid cell of the model along the track. Histograms of sea ice thickness are shown in Figure 6. The simulation with calibrated parameters presents a slightly more realistic sea ice thickness distribution, in particular when sea ice thickness is large. Note that the Operation IceBridge campaigns were conducted essentially in March and over western Arctic sea ice (north of the Canadian Arctic Archipelago and Greenland).

© 2014. American Geophysical Union. All Rights Reserved.

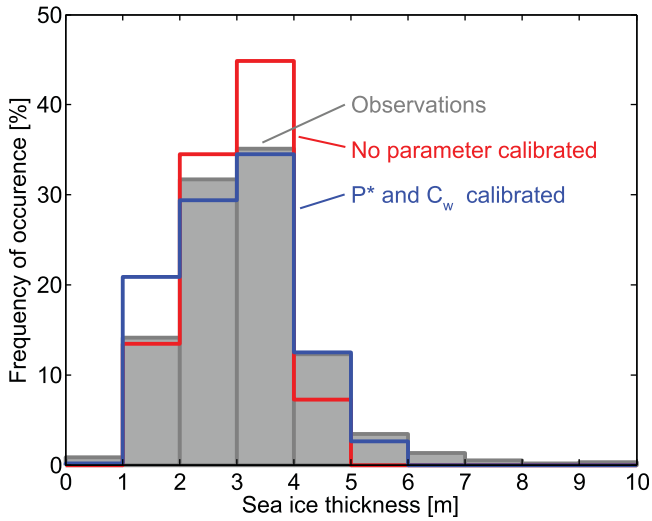

Figure 6. Observed and simulated sea ice thickness distributions. Because of their high spatial frequency, the Operation IceBridge data (gray) [*Kurtz et al.*, 2013] have first been averaged in the corresponding grid cells of the models. We then pick, for each flight campaign between 2009 and 2012, the relevant model sea ice thicknesses (same day and grid cells). Note that the flights from Operation IceBridge cover principally the month of March. In total, 609 data make up the distribution shown here.

4.2.2. Impact on the Areal Sea Ice Distribution

It is expected that the changes in sea ice thickness distribution in winter (Figure 5) affect the ice areal coverage at the end of the melt season, in September. In Figure 7, we plot the 15% isocontours of sea ice concentration from September 2007 to 2012. These contours can in good approximation be interpreted as the ice edge location. We note that the ice edge from the simulation with calibrated parameters lies, with a few exceptions, inside the ice edge of the reference simulation. This is undoubtedly related to the lower sea ice thickness in the calibrated experiment in nearly all the regions, except north of the Canadian Arctic Archipelago, which is a region of perennial ice coverage in all our experiments and in observations. If sea ice is thinner in the majority of the Arctic basin in March (illustrated in Figure 5c), it is also more likely to melt away in the following months. In Baffin Bay, there is usually no ice in September in the observations (Figure 7). NEMO-LIM3 in its reference version does simulate ice in this region. The overestimation of the ice extent in this region is reduced by about 50% after parameter calibration.

Sea ice extent is the sum of all grid cell areas with sea ice concentration larger than 15%. Graphically, it is the surface of the oceanic areas enclosed by the ice edge lines in Figure 7. Sea ice extent for observations and the two simulations are reported within the ice contours of Figure 7. We cannot clearly assess whether or not the simulation with calibrated parameters performs better than the reference simulation. For example, in Figure 7f, the observed record sea ice extent of September 2012 (3.79 million km^2) is closer to observations in the calibrated simulation (3.76 million km^2) than in the reference simulation (4.52 million km^2). In 2009, however, the situation is reversed. Actually, a careful inspection of Figure 7 reveals that the mere change in the two parameters P^* and C_w acts to globally shrink the sea ice pack, but does not guarantee a more realistic spatial distribution of sea ice.

4.2.3. Impact on the Sea Ice Export

We finally look at the simulation of the sea ice areal export through Fram Strait. As stated earlier in the paper (section 2.2), this was the original metric used to tune the model parameters. The monthly simulated sea ice areal exports between 2007 and 2011 are plotted against the Synthetic Aperture Radar (SAR) data of *Kloster and Sandven* [2011] in the scatterplots of Figure 8. As expected, the reference simulation performs well with the dots correctly distributed around the 1-1 line (Figure 8a). The simulation with two calibrated parameters (Figure 8b) overestimates the sea ice export for high values, i.e., in winter. We attribute this overestimation mainly to the global decrease in oceanic drag between the reference and calibrated simulations (C_w from 5.00×10^{-3} to 2.94×10^{-3}). To test this hypothesis, we examined the sea ice export from the experiment with calibrated P^* only (Table 1). This simulation (Figure 8c) shows no visible difference in terms of sea ice areal export and performs as well as the reference simulation.

This example clearly sets the limits of parameter calibration in a global analysis framework, i.e., with one parameter value for the whole model domain. In the EnKF scheme, as in any parameter calibration scheme, the parameters are calibrated for a particular purpose and given the spatial distribution of the observations. Here, we calibrated two parameters based on the simulated sea ice drift with a majority of the data available in the interior of the Arctic basin. Fram Strait only represents a small fraction of the area where data

© 2014. American Geophysical Union. All Rights Reserved.

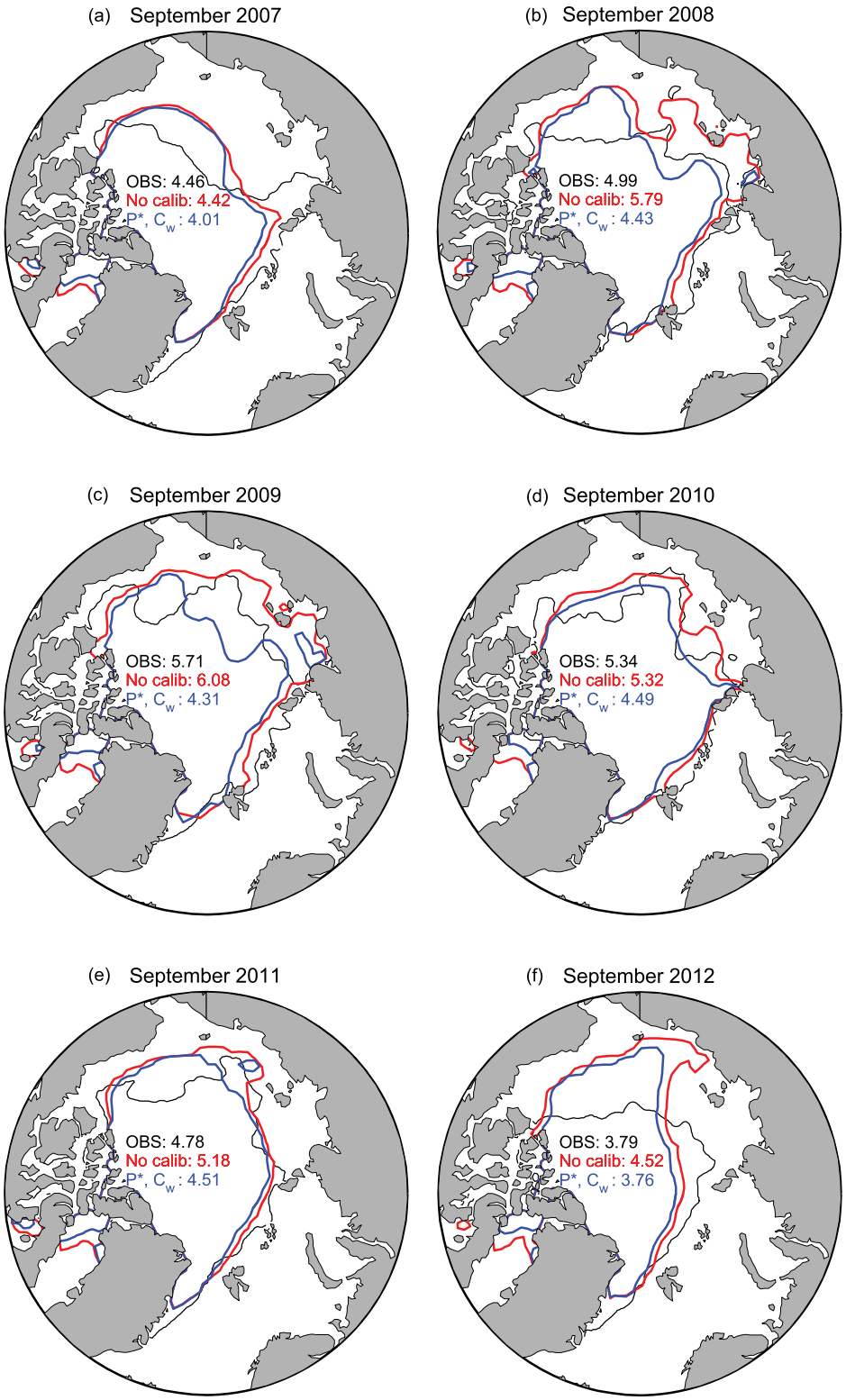

Figure 7. September sea ice edge from 2007 to 2012, defined as the 15% sea ice concentration contour, from observations (black) [*Comiso and Nishio*, 2008], the reference simulation (red), and the simulation with (P^*, C_w) calibrated. The numbers enclosed in the ice edge lines are the sea ice extents, defined as the sum of all grid cell areas with at least 15% of ice. Note that Canadian Arctic Archipelago is excluded from our ice extent computation, as it is not resolved by the ORCA2 grid.

© 2014. American Geophysical Union. All Rights Reserved.

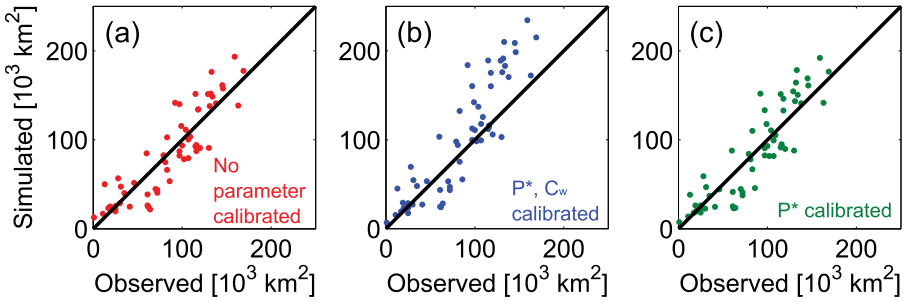

Figure 8. Monthly mean sea ice areal export through Fram Strait, from observations [*Kloster and Sandven*, 2011] and the model with (a) default parameters, (b) (P^*, C_w) calibrated, and (c) P^* calibrated.

were available. By decreasing the oceanic drag coefficient C_w, the EnKF scheme allowed for a better match between simulated and observed sea ice speeds in a large number of grid cells of the Arctic interior, at the expense of a small number of grid points near the ice edge, including Fram Strait.

5. Conclusion

We have presented a simple and efficient method for parameter calibration in large-scale sea ice models. It is based on the classical ensemble Kalman filter (EnKF) equations that we used to perform an analysis of model parameters. A number of 25 members was sufficient to estimate one, two, and three parameters. The method of parameter calibration has two advantages: (1) it respects the model dynamics, in the sense that the new parameter values affect the mean state indirectly (we do not update the state itself when observations are available) and (2) it is entirely objective. It takes about 48 h on 12 CPUs to complete the calibration on a global 2° grid. In terms of CPU resources, this is equivalent to running the model once for about 100 years of simulation. Note that the computational cost required to analyze the parameters is negligible compared to the cost of integrating the ensemble forward.

With only two parameters calibrated (the ice strength parameter P^* and the ocean-sea ice drag parameter C_w), we largely improve the simulation of Arctic sea ice speeds. The new parameter values allow for a globally thinner ice within the basin, and comparison against IceBridge data shows small, but non negligible improvements in the ice thickness distribution with the new parameters. The redistribution in winter sea ice thickness causes in turn a reduction in sea ice areal coverage at the end of the melt season, in September. However, we were not able to assert whether the sea ice areal distribution is better simulated with the calibrated dynamic parameters. Our last metric for evaluation, the areal export of sea ice through Fram Strait, revealed a slight deterioration in winter in the simulation with calibrated parameters. We attributed this deterioration to the small weight given to this region in the overall procedure of parameter calibration.

While the method of parameter calibration with the EnKF is attractive, its results cannot be overinterpreted. It is vain to think of parameter calibration as a method for finding hypothetically true values of parameters that actually exist in the real world. In different sea ice models with the same quadratic air drag parameterization, the value of optimal atmospheric drag often strongly varies [*Miller et al.*, 2006]. *Feltham* [2008] points out that the value for P^* is frequently tuned within a factor of 10. The reason is simple: the optimal set of parameters for a given configuration is a function of several factors: the initial and boundary conditions, the resolution, the physics of the model, and the type and availability of data used to constrain the parameters [*Miller et al.*, 2006; *Nguyen et al.*, 2011]. In other words, the calibration is an opportunity to transfer uncertainty from various sources, including model errors, on a set of loosely constrained parameters. The values of parameters that we ultimately end with ($P^* = 0.98 \times 10^4 \mathrm{N/m^2}$ and $C_w = 2.94 \times 10^{-3}$) should thus be thought as optimal values for the ocean-sea ice model NEMO-LIM3, at 2° resolution, with the atmospheric forcing from NCEP/NCAR, for the Arctic, between 2007 and 2012, and for the simulation of sea ice drift between October and April where observations were available. It would therefore not be wise to recommend these values to other sea ice modelers, simply because their configuration will be necessarily different. In fact, the step of parameter calibration presented in this paper should be repeated whenever the model configuration changes.

© 2014. American Geophysical Union. All Rights Reserved.

The parameter calibration with the EnKF can be extended to more general configurations, including climate GCMs. A time-evolving estimate of optimal parameters can be obtained by maintaining the spread of the ensemble adequately. This could be particularly relevant for hindcasting or reanalyzes purposes, as the optimal set of sea ice parameters may actually be changing while sea ice itself is experiencing thinning. It is also technically possible to estimate spatially varying parameters. However such spatial parameter estimation would raise other challenges. First, estimation of P^* is mainly related to the ice properties, which are advecting with time. Thus, in case of spatial estimation of parameters, one should advect the parameter estimated with the rest of the ice characteristics in the sea ice model. Second, uniform ensemble inflation is failing with heterogeneous observation networks [*Anderson*, 2001] and other approaches must be considered to maintain ensemble spread, e.g., additive inflation [*Evensen*, 2007] or inflation-free methods [e.g., *Bocquet and Sakov*, 2012]. We could also make use of other several observational products than sea ice drift, and therefore increase the number of parameters to calibrate. But, as illustrated in this paper, the choice of parameters for estimation should be made after close examination of the internal dynamics of the system: calibrating interdependent parameters is not a guarantee for better model performance.

The objective calibration of parameters is without doubt an improvement compared to the subjective and often not documented methods generally applied. The calibration of parameters remains a critical and important step in large-scale sea ice models, and to a larger extent in global climate models. As it has the potential to significantly affect the model climate, this step should not be underestimated in the process of model development. Because the number of possible combinations grows exponentially with the number of parameters to be adjusted, ensemble methods for parameter calibration, such as the one presented in this paper, represent promising opportunities to identify and reduce the model biases in a systematic way.

Acknowledgments
We thank two anonymous reviewers for their helpful comments that permitted to improve the manuscript. We thank T. Lavergne, P. Rampal, S. Bouillon, and L. Bertino for helpful discussions. O. Lecomte is acknowledged for the postprocessing of Operation IceBridge data. François Massonnet is a F.R.S.-FNRS Research Fellow. Hugues Goosse is a F.R.S.-FNRS Senior Research Associate. This work was partly funded by the European Commissions 7th Framework Programme, COMBINE project under grant Agreement 226520 (Comprehensive Modelling of the Earth System for Better Climate Prediction and Projection) and the SANGOMA project, under grant 283580 (Stochastic Assimilation for the Next Generation Ocean Model Applications). It was also partly supported by the Belgian Science Federal Policy Office (BELSPO).

References

Anderson, J. L. (2001), An ensemble adjustment Kalman filter for data assimilation, *Mon. Weather Rev.*, *129*(12), 2884–2903, doi:10.1175/1520-0493(2001)129<2884:AEAKFF>2.0.CO;2.

Annan, J. D., D. J. Lunt, J. C. Hargreaves, and P. J. Valdes (2005), Parameter estimation in an atmospheric GCM using the Ensemble Kalman Filter, *Nonlinear Processes Geophys.*, *12*(3), 363–371, doi:10.5194/npg-12-363-2005.

Baumgartner, A., and E. Reichel (1976), The world water balance mean annual global, continental and maritime precipitation, evaporation and run-off, *Agric. Water Manage.*, *1*(1), 100–101. [Available at http://ideas.repec.org/a/eee/agiwat/v1y1976i1p100-101.html.]

Beckmann, A., and R. Döscher (1997), A method for improved representation of dense water spreading over topography in geopotential-coordinate models, *J. Phys. Oceanogr.*, *27*(4), 581–591, doi:10.1175/1520-0485(1997)027<0581:AMFIRO>2.0.CO;2.

Berliand, M. E., and T. G. Strokina (1980), *Global Distribution of the Total Amount of Clouds*, 71 pp., Hydrometeorological, Leningrad, Russia.

Blanke, B., and P. Delecluse (1993), Variability of the tropical Atlantic Ocean simulated by a general circulation model with two different mixed-layer physics, *J. Phys. Oceanogr.*, *23*(7), 1363–1388, doi:10.1175/1520-0485(1993)023<1363:VOTTAO>2.0.CO;2.

Bocquet, M. (2011), Ensemble Kalman filtering without the intrinsic need for inflation, *Nonlinear Processes Geophys.*, *18*(5), 735–750, doi:10.5194/npg-18–735-2011.

Bocquet, M., and P. Sakov (2012), Combining inflation-free and iterative ensemble kalman filters for strongly nonlinear systems, *Nonlinear Processes Geophys.*, *19*, 383–399, doi:10.5194/npg-19–383-2012.

Bougeault, P., and P. Lacarrere (1989), Parameterization of orography-induced turbulence in a mesobeta–scale model, *Mon. Weather Rev.*, *117*(8), 1872–1890, doi:10.1175/1520-0493(1989)117<1872:POOITI>2.0.CO;2.

Bouillon, S., M. A. Morales Maqueda, V. Legat, and T. Fichefet (2009), An elastic-viscous-plastic sea ice model formulated on Arakawa B and C grids, *Ocean Modell.*, *27*, 174–184.

Burgers, G., P. van Leeuwen, and G. Evensen (1998), Analysis scheme in the ensemble Kalman filter, *Mon. Weather Rev.*, *126*(6), 1719–1724, doi:10.1175/1520-0493(1998)126<1719:ASITEK>2.0.CO;2.

Chevallier, M., and D. Salas Mélia (2012), The role of sea ice thickness distribution in the Arctic sea ice potential predictability: A diagnostic approach with a coupled GCM, *J. Clim.*, *25*, 3025–3038.

Comiso, J. C., and F. Nishio (2008), Trends in the sea ice cover using enhanced and compatible AMSR-E, SSM/I and SMMR data, *J. Geophys. Res.*, *113*, C02S07, doi:10.1029/2007JC004257.

Dorn, W., K. Dethloff, A. Rinke, S. Frickenhaus, R. Gerdes, M. Karcher, and F. Kauker (2007), Sensitivities and uncertainties in a coupled regional atmosphere-ocean-ice model with respect to the simulation of Arctic sea ice, *J. Geophys. Res.*, *112*, D10118, doi:10.1029/2006JD007814.

Evensen, G. (2003), The ensemble Kalman filter: Theoretical formulation and practical implementation, *Ocean Dyn.*, *53*, 343–367.

Evensen, G. (2007), *Data Assimilation—The Ensemble Kalman Filter*, Springer, N. Y.

Feltham, D. L. (2008), Sea ice rheology, *Annu. Rev. Fluid Mech.*, *40*(1), 91–112, doi:10.1146/annurev.fluid.40.111406.102151.

Fichefet, T., and M. A. Morales Maqueda (1997), Sensitivity of a global sea ice model to the treatment of ice thermodynamics and dynamics, *J. Geophys. Res.*, *102*, 12,609–12,646.

Fischer, H., and P. Lemke (2013), On the required accuracy of atmospheric forcing fields for driving dynamic-thermodynamic sea ice models, in *The Polar Oceans and Their Role in Shaping the Global Environment*, pp. 373–381, AGU, Washington, D. C., doi:10.1029/GM085p0373.

Girard, L., J. Weiss, J. M. Molines, B. Barnier, and S. Bouillon (2009), Evaluation of high-resolution sea ice models on the basis of statistical and scaling properties of Arctic sea ice drift and deformation, *J. Geophys. Res.*, *114*, C08015, doi:10.1029/2008JC005182.

Girard, L., S. Bouillon, J. Weiss, D. Amitrano, T. Fichefet, and V. Legat (2011), A new modeling framework for sea-ice mechanics based on elasto-brittle rheology, *Ann. Glaciol.*, *52*(57), 123–132.

 © 2014. American Geophysical Union. All Rights Reserved.

Goosse, H. (1997), Modelling the large-scale behaviour of the coupled ocean-sea-ice system, PhD thesis, Université catholique de Louvain.
Goosse, H., and T. Fichefet (1999), Importance of ice-ocean interactions for the global ocean circulation: A model study, *J. Geophys. Res.*, *104*, 23,337–23,355.
GRDC (2000), Observed historical discharge data from major rivers for climate model validation, *Tech. Rep. 307*, Max Planck Inst., Hamburg, Germany. [Available at https://www.mpimet.mpg.de/fileadmin/publikationen/Reports/max_scirep_307.pdf.]
Harder, M., and H. Fischer (1999), Sea ice dynamics in the Weddell Sea simulated with an optimized model, *J. Geophys. Res.*, *104*, 11,151–11,162, doi:10.1029/1999JC900047.
Hibler, W. D. (1979), A dynamic thermodynamic sea ice model, *J. Phys. Oceanogr.*, *9*, 815–846.
Hunke, E. C., and J. K. Dukowicz (1997), An elastic-viscous-plastic model for sea ice dynamics, *J. Phys. Oceanogr.*, *27*, 1849–1867.
Hunke, E. C., W. H. Lipscomb, and A. K. Turner (2010), Sea ice models for climate study: Retrospective and new directions, *J. Glaciol.*, *56*, 1162–1172.
Jazwinski, A. H. (1970), *Stochastic Processes and Filtering Theory*, Academic, N. Y.
Juricke, S., P. Lemke, R. Timmermann, and T. Rackow (2012), Effects of stochastic ice strength perturbation on Arctic finite element sea ice modeling, *J. Clim.*, *26*(11), 3785–3802, doi:10.1175/JCLI-D-12-00388.1.
Kalnay, E., et al. (1996), The NCEP/NCAR 40-year reanalysis project, *Bull. Am. Meteorol. Soc.*, *77*, 437–471.
Keghouche, I. (2010), Modeling the dynamics and drift of icebergs in the Barents Sea, PhD thesis, Univ. of Bergen, Bergen, Norway.
Kim, J. G., E. C. Hunke, and W. H. Lipscomb (2006), Sensitivity analysis and parameter tuning scheme for global sea-ice modeling, *Ocean Modell.*, *14*, 61–80.
Kloster, K., and S. Sandven (2011), Ice motion and ice area flux in Fram Strait at 79N using ASAR and passive microwave for Feb. 2004 Jul. 2010, *Tech. Rep. 322*, Nansen Environ. and Remote Sens. Cent., Bergen, Norway. [Available at http://arctic-roos.org/Members/nguest/monitoring-sea-ice-area-flux-in-the-fram-strait-using-satellite-sar-data-nersc.]
Kurtz, N. T., S. L. Farrell, M. Studinger, N. Galin, J. P. Harbeck, R. Lindsay, V. D. Onana, B. Panzer, and J. G. Sonntag (2013), Sea ice thickness, freeboard, and snow depth products from Operation IceBridge airborne data, *Cryosphere*, *7*(4), 1035–1056, doi:10.5194/tc-7-1035-2013.
Large, W. G., and S. G. Yeager (2004), Diurnal to decadal global forcing for ocean and sea-ice models: The data sets and flux climatologies, technical report NCAR (National Center for Atmospheric Research)/TN-460+STR, Boulder, Colo.
Lavergne, T., S. Eastwood, Z. Teffah, H. Schyberg, and L.-A. Breivik (2010), Sea ice motion from low-resolution satellite sensors: An alternative method and its evaluation in the Arctic, *J. Geophys. Res.*, *115*, C10032, doi:10.1029/2009JC005958.
Leppäranta, M. (2005), *The Drift of Sea Ice*, Springer, N. Y.
Levitus, S. (1998), *NODC World Ocean Atlas*. [Available at http://www.esrl.noaa.gov/psd/.], National Oceanic and Atmospheric Administration (NOAA), Washington, D. C.
Lisæter, K. A., J. Rosanova, and G. Evensen (2003), Assimilation of ice concentration in a coupled ice-ocean model, using the Ensemble Kalman filter, *Ocean Dyn.*, *53*, 368–388, doi:10.1007/s10236-003-0049-4.
Lisæter, K. A., G. Evensen, and S. Laxon (2007), Assimilating synthetic CryoSat sea ice thickness in a coupled ice-ocean, *J. Geophys. Res.*, *112*, C07023, doi:10.1029/2006JC003786.
Madec, G. (2008), *NEMO Ocean Engine: Note du Pôle de Modélisation*, vol. 27, Inst. Pierre-Simon Laplace, France. [Available at http://www.nemo-ocean.eu/About-NEMO/Reference-manuals.]
Maslanik, J., T. Agnew, M. Drinkwater, W. Emery, C. Fowler, R. Kwok, and A. Liu (1998), Summary of ice-motion mapping using passive microwave data, technical report number 8, National Snow and Ice Data Center (NSIDC), Boulder, Colo. [Available at http://nsidc.org/pubs/special/.]
Massonnet, F., T. Fichefet, H. Goosse, M. Vancoppenolle, P. Mathiot, and C. König Beatty (2011), On the influence of model physics on simulations of Arctic and Antarctic sea ice, *The Cryosphere*, *5*(3), 687–699, doi:10.5194/tc-5-687-2011. [Available at http://www.the-cryosphere.net/5/687/2011/.]
Massonnet, F., P. Mathiot, T. Fichefet, H. Goosse, C. König Beatty, M. Vancoppenolle, and T. Lavergne (2013), A model reconstruction of the Antarctic sea ice thickness and volume changes over 1980–2008 using data assimilation, *Ocean Modell.*, *64*, 67–75, doi:10.1016/j.ocemod.2013.01.003.
Mathiot, P., C. König Beatty, T. Fichefet, H. Goosse, F. Massonnet, and M. Vancoppenolle (2012), Better constraints on the sea-ice state using global sea-ice data assimilation, *Geosci. Model Dev.*, *5*(6), 1501–1515, doi:10.5194/gmd-5-1501-2012.
Mauritsen, T., et al. (2012), Tuning the climate of a global model, *J. Adv. Model. Earth Syst.*, *4*, M00A01, doi:10.1029/2012MS000154.
McPhee, M. (1980), An analysis of pack ice drift in summer, in *Sea Ice Processes and Models*, edited by R. Pritchard, pp. 62–75, Univ. of Wash., Seattle.
Miller, P. A., S. W. Laxon, D. L. Feltham, and D. J. Cresswell (2006), Optimization of a sea ice model using basinwide observations of Arctic sea ice thickness, extent and velocity, *J. Clim.*, *19*, 1090–1108.
Nguyen, A. T., D. Menemenlis, and R. Kwok (2011), Arctic ice-ocean simulation with optimized model parameters: Approach and assessment, *J. Geophys. Res.*, *116*, C04025, doi:10.1029/2010JC006573.
Notz, D. (2012), Challenges in simulating sea ice in earth system models, *WIREs Clim. Change*, *3*(6), 509–526, doi:10.1002/wcc.189.
Owens, W. B., and P. Lemke (1990), Sensitivity studies with a sea ice-mixed layer-pycnocline model in the Weddell Sea, *J. Geophys. Res.*, *95*, 9527–9538, doi:10.1029/JC095iC06p09527.
Rae, J., H. Hewitt, A. Keen, J. Ridley, J. Edwards, and C. Harris (2014), A sensitivity study of the sea ice simulation in the global coupled climate model, hadgem3, *Ocean Modell.*, *74*, 60–76, doi:10.1016/j.ocemod.2013.12.003.
Rampal, P., J. Weiss, D. Marsan, and M. Bourgoin (2009), Arctic sea ice velocity field: General circulation and turbulent-like fluctuations, *J. Geophys. Res.*, *114*, C10014, doi:10.1029/2008JC005227.
Sakov, P., and P. R. Oke (2008), A deterministic formulation of the ensemble Kalman filter: An alternative to ensemble square root filters, *Tellus, Ser. A*, *60*, 361–371.
Shine, K. P., and A. Henderson-Sellers (1985), The sensitivity of a thermodynamic sea ice model to changes in surface albedo parameterization, *J. Geophys. Res.*, *90*, 2243–2250.
Steele, M., J. Zhang, D. Rothrock, and H. Stern (1997), The force balance of sea ice in a numerical model of the arctic ocean, *J. Geophys. Res.*, *102*, 21,061–21,079, doi:10.1029/97JC01454.
Stössel, A. (1992), Sensitivity of Southern Ocean sea-ice simulations to different atmospheric forcing algorithms, *Tellus, Ser. A*, *44*(5), 395–413, doi:10.1034/j.1600-0870.1992.t01-3-00004.x.
Stössel, A., P. Lemke, and W. B. Owens (1990), Coupled sea ice-mixed layer simulations for the Southern Ocean, *J. Geophys. Res.*, *95*, 9539–9555, doi:10.1029/JC095iC06p09539.

 © 2014. American Geophysical Union. All Rights Reserved.

Sumata, H., F. Kauker, R. Gerdes, C. Köberle, and M. Karcher (2013), A comparison between gradient descent and stochastic approaches for parameter optimization of a sea ice model, *Ocean Sci.*, *9*(4), 609–630, doi:10.5194/os-9-609-2013.
Thomas, D., and G. Dieckmann (2010), *Sea Ice*, Wiley, Oxford, U. K.
Thorndike, A. S. (1986), Diffusion of sea ice, *J. Geophys. Res.*, *91*, 7691–7696, doi:10.1029/JC091iC06p07691.
Thorndike, A. S., D. A. Rothrock, G. A. Maykut, and R. Colony (1975), The thickness distribution of sea ice, *J. Geophys. Res.*, *80*, 4501–4513.
Trenberth, K. E., W. Large, and European Centre for Medium Range Weather Forecasts (1989), A global ocean wind stress climatology based on the ECMWF analyses. [Available at http://dss.ucar.edu/datasets/ds110.1/.], National Center for Atmospheric Research (NCAR), Boulder, Colo.
Uotila, P., S. OFarrell, S. Marsland, and D. Bi (2012), A sea-ice sensitivity study with a global ocean-ice model, *Ocean Modell.*, *51*, 1–18, doi:10.1016/j.ocemod.2012.04.002.
Vancoppenolle, M., T. Fichefet, H. Goosse, S. Bouillon, G. Madec, and M. A. Morales Maqueda (2009), Simulating the mass balance and salinity of Arctic and Antarctic sea ice. 1. Model description and validation, *Ocean Modell.*, *27*, 33–53.
Vancoppenolle, M., et al. (2013), Role of sea ice in global biogeochemical cycles: Emerging views and challenges, *Quat. Sci. Rev.*, *79*, 207–230, doi:10.1016/j.quascirev.2013.04.011.

© 2014. American Geophysical Union. All Rights Reserved.